A Preliminary Foil Gas Bearing Performance Map

Christopher DellaCorte
Glenn Research Center, Cleveland, Ohio

Kevin C. Radil
U.S. Army Research Laboratory, Glenn Research Center, Cleveland, Ohio

Robert J. Bruckner and S. Adam Howard
Glenn Research Center, Cleveland, Ohio

NASA STI Program . . . in Profile

Since its founding, NASA has been dedicated to the advancement of aeronautics and space science. The NASA Scientific and Technical Information (STI) program plays a key part in helping NASA maintain this important role.

The NASA STI Program operates under the auspices of the Agency Chief Information Officer. It collects, organizes, provides for archiving, and disseminates NASA's STI. The NASA STI program provides access to the NASA Aeronautics and Space Database and its public interface, the NASA Technical Reports Server, thus providing one of the largest collections of aeronautical and space science STI in the world. Results are published in both non-NASA channels and by NASA in the NASA STI Report Series, which includes the following report types:

- TECHNICAL PUBLICATION. Reports of completed research or a major significant phase of research that present the results of NASA programs and include extensive data or theoretical analysis. Includes compilations of significant scientific and technical data and information deemed to be of continuing reference value. NASA counterpart of peer-reviewed formal professional papers but has less stringent limitations on manuscript length and extent of graphic presentations.

- TECHNICAL MEMORANDUM. Scientific and technical findings that are preliminary or of specialized interest, e.g., quick release reports, working papers, and bibliographies that contain minimal annotation. Does not contain extensive analysis.

- CONTRACTOR REPORT. Scientific and technical findings by NASA-sponsored contractors and grantees.

- CONFERENCE PUBLICATION. Collected papers from scientific and technical conferences, symposia, seminars, or other meetings sponsored or cosponsored by NASA.

- SPECIAL PUBLICATION. Scientific, technical, or historical information from NASA programs, projects, and missions, often concerned with subjects having substantial public interest.

- TECHNICAL TRANSLATION. English-language translations of foreign scientific and technical material pertinent to NASA's mission.

Specialized services also include creating custom thesauri, building customized databases, organizing and publishing research results.

For more information about the NASA STI program, see the following:

- Access the NASA STI program home page at *http://www.sti.nasa.gov*

- E-mail your question via the Internet to *help@sti.nasa.gov*

- Fax your question to the NASA STI Help Desk at 301–621–0134

- Telephone the NASA STI Help Desk at 301–621–0390

- Write to:
  NASA STI Help Desk
  NASA Center for AeroSpace Information
  7121 Standard Drive
  Hanover, MD 21076–1320

A Preliminary Foil Gas Bearing Performance Map

Christopher DellaCorte
Glenn Research Center, Cleveland, Ohio

Kevin C. Radil
U.S. Army Research Laboratory, Glenn Research Center, Cleveland, Ohio

Robert J. Bruckner and S. Adam Howard
Glenn Research Center, Cleveland, Ohio

National Aeronautics and
Space Administration

Glenn Research Center
Cleveland, Ohio 44135

October 2006

Level of Review: This material has been technically reviewed by technical management.

A Preliminary Foil Gas Bearing Performance Map

Christopher DellaCorte
National Aeronautics and Space Administration
Glenn Research Center
Cleveland, Ohio 44135

Kevin C. Radil
U.S. Army Research Laboratory
Glenn Research Center
Cleveland, Ohio 44135

Robert J. Bruckner and S. Adam Howard
National Aeronautics and Space Administration
Glenn Research Center
Cleveland, Ohio 44135

Abstract

Recent breakthrough improvements in foil gas bearing load capacity, high temperature tribological coatings and computer based modeling have enabled the development of increasingly larger and more advanced Oil-Free Turbomachinery systems. Successful integration of foil gas bearings into turbomachinery requires a step wise approach that includes conceptual design and feasibility studies, bearing testing, and rotor testing prior to full scale system level demonstrations. Unfortunately, the current level of understanding of foil gas bearings and especially their tribological behavior is often insufficient to avoid developmental problems thereby hampering commercialization of new applications. In this paper, a new approach loosely based upon accepted hydrodynamic theory, is developed which results in a "Foil Gas Bearing Performance Map" to guide the integration process. This performance map, which resembles a Stribeck curve for bearing friction, is useful in describing bearing operating regimes, performance safety margins, the effects of load on performance and limiting factors for foil gas bearings.

Introduction

Foil gas bearings are compliant surface, self-acting hydrodynamic bearings that use ambient gas as their working fluid. They do not require external pressurization and are typically constructed from several layers of sheet metal foils from which they derive their name: (1) Figure 1 shows examples of early style journal bearings. Foil bearings are in widespread commercial use in air cycle machines employed to pressurize aircraft cabins, in turbocompressors and turboexpanders and in some microturbine generator systems. (2) These successful systems were deployed largely through experimentally based trial and error programs. In the earliest applications, foil air bearings were abruptly transitioned from the lab directly to system level demonstrations often accompanied with repeated failures. (3) More recently, the authors have been advocating a four step process for the development of Oil-Free Turbomachinery systems in which each successive step builds upon the information gained in previous, less complex steps. The process is briefly reviewed here and is described in greater detail in the literature (4).

The first step in developing a new, foil bearing supported rotor system is to conduct a rotor layout and conceptual design feasibility study. During this preliminary step, bearing loads, performance requirements and shaft geometrical layout trade studies are conducted. Once a suitable preliminary rotor design is established for which bearing requirements like load capacity, stiffness and damping, orbit control etc., fall within acceptable limits, the next step is bearing design and testing. In the second step, bearings are designed that meet the performance criteria determined in step one and then manufactured and tested in

laboratory test rigs. Verification tests on bearing lift-off speed, load capacity, power loss and rudimentary dynamic characterization are conducted. If the bearings are capable of meeting the rotor support requirements developed in the first two steps, the bearings are transitioned into step three and tested on a rotordynamic simulator rig.

This third step utilizes a physical mock-up of the system rotor (shaft) in which the mass and inertial properties of the real system are matched to the greatest extent possible but employ dummy masses for bladed components, that is, the compressor and turbine wheels. In this rotordynamic rig, multiple bearings are tested to determine if they can control the orbit satisfactorily. Also during this testing, the bearing's nominal stiffness and damping properties can be estimated and compared to those expected. Following successful completion of the rotor simulation, the fourth and final step is a full scale system level demonstration.

These four steps are considered the minimum process to mitigate development risk. In practice, the process is iterative. Failure to meet objectives in one step usually requires more work at lower level steps prior to system demonstration. The shortcoming of this four step process is that it does not yield information regarding an envelope of operating conditions over which the rotor system, or more specifically the foil bearings, can survive. Put another way, the four step method reduces risk of demonstration failures but does not provide an understanding of the robustness of the design. Further, for any given operating condition, there exists little or no way of determining how much of a safety margin the bearings have with respect to failure. One approach to determine robustness is to produce multiple rotors with varying geometries to determine bearing operating limits. This brute force, hardware intensive path, however, is costly. A new, less hardware intensive approach is needed to evaluate system level foil bearing robustness which takes into account existing available empirical and analytical foil bearing modeling. The current paper does just this and builds upon earlier modeling work on bearing load capacity.

Nomenclature

A	First Coefficient in the power loss relationship, W/mm^2, (W/in.^{2})
B	Second Coefficient in the power loss relationship, W/(mm^2 N^2), (W/in.^{2} lb^2)
$B_\#$	Coefficient in the high speed torque and friction coefficient approximation
$\mathcal{D}$	Foil Bearing performance coefficient, N/(mm^3 krpm), (lb/(in.^{3} krpm))
D	Diameter of bearing shaft, mm (in.)
f	Coefficient of friction
η	Dynamic viscosity, kg/(m s), (lbm/(ft s))
η_o	Dynamic viscosity of air at standard, sea-level conditions
L	Axial length of bearing, mm (in.)
R_o	Radius of the journal, mm (in.)
S'	Modified Sommerfeld number
P_l'	Area specific power loss, W/mm^2 (W/in.^{2})
Ω_k	Shaft rotational speed, krpm
W_t	Total bearing load, N (lb)
T	Bearing torque, N-m (ft-lb)

Foil Bearing Models

DellaCorte and Valco published a foil bearing load capacity estimation method in a 2001 paper (ref. 5). With this approach, the load capacity of foil air bearings is calculated based upon a simple linear equation which incorporates the bearing size (area), surface velocity and an empirically determined "load capacity coefficient", $\mathcal{D}$. In the paper, this coefficient was related to the stiffness complexity of the foil spring understructure. Simple bearing designs in which the top foil stiffness is uniform yielded load

capacities roughly one third that of more modern designs in which the stiffness was spatially varied in more than one direction. The availability of this simple "Rule-of-Thumb" for foil bearing load capacity greatly aids the bearing sizing task encompassed by step one in the four step process. The scope of the load capacity model is limited. More analytically based design guidance is needed especially, for example, in determining system thermal stability and bearing power loss.

Recent publications on foil bearing performance (refs. 6 to 8) clearly show that thermal management of foil bearings is critical to sustained operation even while airborne when friction is low. Dykas and Howard (ref. 6), for instance, analyzed repeated bearing failures that resulted in high speed seizures and melted shafts. Their analyses concluded that insufficient thermal management combined with geometrical shaft wall thickness variations led to the unexpected thermal runaway failure. One systematic study demonstrated that ineffective thermal management can lead to preferential shaft expansion resulting in a tightening effect on the bearings (ref. 9). Based upon these and other findings, it is apparent that in foil bearings, localized overheating and thermal gradients can lead to foil distortions which are larger than the gas film thickness. This thermal run-away scenario is a significant cause of foil bearing failure. Unfortunately, no adequate method exists for designers to judge the available engineering safety margin of a particular bearing-rotor-system design.

The current method to mitigate thermal run-away is to maximize convective thermal stabilization by bleeding excess gas around the bearings. This, however, depletes the machine of valuable pressurized working fluid causing an overall loss in efficiency. A better systems level understanding of power loss can facilitate the use of foil bearings in their low power loss regime, hence reducing the need for bleed gas. To overcome this problem a new foil bearing operating map is proposed. This map, which relates bearing power loss to its operating condition, is intended to supplement the four step design process and can be applied iterative and repeatedly at each step.

Foil Bearing Operating Map Development

The proposed foil bearing operating map is analogous to the well known compressor operating map used by turbomachinery designers to judge safety margins between discharge pressure and mass flow operating conditions to choked or stalled flow conditions. Figure 2 shows a sketch of a typical compressor map adapted from the literature (ref. 10). By pin-pointing a unique map location, one can determine a compressor's operating condition and safety margin with respect to, for instance, stall or choked flow. Performance and operability parameters such as mass flow, pressure rise, efficiency, and power requirements are captured by this approach. Safety parameters such as stall margin, flow range, speed sensitivity, and flow distortion severity also become apparent from the map. A similar map approach for turbines has also been developed and their combined effect has been to successfully facilitate the design and development of high speed turbomachinery products. The proposed map for foil bearings, qualitatively, follows an analogous approach but using different parameters.

For foil bearings, power loss is used in place of compressor pressure ratio and a modified form of the Sommerfeld number, which relates hydrodynamic pressure to an equivalent bearing unit load, is proposed for use in place of a compressor mass flow rate. By adopting this graphical technique, one can plot various regions where good performance can be expected and regions where bearing operation may not be possible, such as at very high power loss levels where thermal stability would be difficult to achieve. Figure 3 shows the axes of the proposed foil bearing operating map and the physical meaning of the axis parameters.

Earlier investigations in fluid film bearing friction and power loss offer guidance in developing the approach used in this paper. Lu and Khonsari, for instance, recently published a paper on the use of the Stribeck curve and related analytical relations to predict the lift-off speed and friction in oil-lubricated journal bearings (ref. 11). In their paper they noted that the Stribeck approach, in which bearing friction is related to the Sommerfeld number, has been applied to many lubricated contacts. It has not, however, to the authors' knowledge been applied to compliant surface foil gas bearings. To better understand foil gas

bearings, we have chosen to utilize the Stribeck approach but modify the parameters to encompass foil bearing specific characteristics.

For the foil bearing operating map, the well known Sommerfeld number, S, is altered to include the ratio of gas viscosity to the viscosity of air at standard conditions, the foil bearing load capacity coefficient empirically determined as in reference 5, the bearing surface velocity and the total specific load on the bearing comprised of deadweight, any dynamic loads, spring preloads, and loads due to centrifugal and thermal expansion growth of the shaft into the foil bearing. The equation is shown below

$$S' = \frac{\eta}{\eta_o} \frac{\mathcal{D}(D\Omega_k)}{W_t/DL} \approx \frac{hydrodynamic\ pressure}{area\ specific\ load} \qquad (1)$$

Essentially, the numerator is a measure of the gas pressure generated in the film and the denominator is a measure of the forces per unit area acting against the hydrodynamic pressure. The value of this parameter largely dictates the amount of stress the bearing is under. Low values of S' indicate a highly loaded, low speed bearing and high values are representative of lightly loaded, high speed bearings. Prior to plotting empirical data for a foil bearing and revealing the nature of this map, it is instructive to discuss the factors which provide limits or boundaries to foil bearing supported systems.

The lubricating gas, often ambient air, is used for bearing thermal management or cooling. Since the thermal capacity of air is relatively low compared to conventional hydrodynamic lubricants like oil, its ability to carry heat (e.g., due to friction) out of a bearing is limited. Excessive heat generation or inadequate cooling can result in thermally induced seizure and bearing failure and thus overheating represents a boundary or thermal limit to foil bearing operation. Experience has shown that when foil bearing power loss exceeds $0.015\ W/mm^2$ ($100\ W/in.^2$) of bearing projected area, failure through thermally induced distortion is a strong possibility (refs. 12 and 13). Thus, the ordinate or vertical axis of the map extends to a value near $100\ W/in.^2$. Further, power dissipated in the gas film is always positive; the minimum specific power loss value is zero (see fig. 4).

On the abscissa, there are two limits, one at the low end and one at the high end of the axis. The modified Sommerfeld number, S', is largely comprised of the bearing load capacity divided by the load and thus realistically cannot exist in steady state conditions below a value of 1.0 because operating a bearing above its load capacity (S'<1) is not possible. This fact establishes a lower practical limit for S'. On the other hand, S' cannot be infinite.

The shafts or journals against which foil bearings operate have strength/weight ratios which limit high speed operation. If it is assumed that journal shafts are made from high strength superalloys, maximum surface velocities are typically 500 m/s or less to avoid burst failure. Similar strength limits exist for thrust runners operating against thrust foil bearings. Combined with measured load capacity coefficients between 0.25 and 1.0, fairly constant gas viscosity properties and static loading rarely less than ~15 kPa (2 psi) (deadweight plus small shaft growth), S' values appear to be limited to about 150. Operating points within these described boundaries capture foil bearings in use today and into the near foreseeable future. Figure 5 shows the foil bearing operating map with these additional limits and represents the operating space for foil gas bearings.

Power Loss Measurement

The ordinate of the operating map is the measured bearing power loss divided by the bearing's projected area (length multiplied by diameter). This could also be called the specific power loss and has units of watts per square millimeter (in.). This parameter serves as a crude measure of the thermal stress on a bearing. It also represents the heat flux that must be managed during foil bearing operation. Heat is generated through shearing of the gas film and this heat, if not carried away by cooling air or conduction into the shaft, can lead to geometrical distortion of the foil and shaft and ultimately to bearing failure.

The power loss is calculated as the bearing torque multiplied by the angular velocity of the bearing in radians per second. The bearing torque is experimentally measured utilizing a foil bearing test rig shown in figure 6. With this rig, a foil bearing is loaded against a shaft using a set of uniformly distributed donut-shaped weights. Bearing torque, sometimes referred to as friction, is measured with a calibrated force transducer. A more complete description of this test set-up has been previously published (ref. 14). Other means to load the bearing, such as cables and actuators, are not employed as these techniques have a tendency to introduce inaccuracies to the friction measurements. Since the hydrodynamic friction of an operating foil bearing can be quite low, every precaution must be taken to ensure accurate torque measurements.

Modified Sommerfeld (S') Determination

As shown in equation (1), the S' number is dimensionless but includes a number of constants and experimentally determined parameters. If, for the present discussion, we only consider air lubricated foil bearings operating at ambient pressure (one atmosphere), the viscosity ratio term is unity and can be ignored. The load capacity coefficient, $\mathcal{D}$, can be estimated from the foil bearing structural design as described in reference 5 or experimentally measured during high load testing as outlined in reference 15. This coefficient typically ranges from 0.25 to 1.0. The shaft speed is directly measured during the bearing friction testing and requires no further explanation. The total specific bearing load, which essentially makes up the denominator of the parameter, is a bit more complex.

The total specific load parameter captures the stresses placed on the gas film by the bearing and the shaft. This includes deadweight loading, initial bearing spring preload, centrifugal and thermal growth of the shaft deflecting the bearing spring structure, dynamic loading due to vibration and mechanical run-out, and bearing loading due to misalignment. There may be other stressors on the lubricating gas film as well that have not yet been characterized but can be added later. Further, at this preliminary stage of map development, it is not clear that it is correct to algebraically add these loads together. For example, deadweight and dynamic loads are directional and act upon only one section or region of a bearing at one time. Other loads, such as those which are from thermal and centrifugal shaft growth are more uniformly distributed around the bearing.

To simplify this preliminary model development and collect useful data, experiments were performed that carefully minimized or controlled as many of these load factors as possible. For instance, the deadweight is measured. The spring preload, which is typically 2 to 7 kPa (0.25 to 1.0 psi) for foil bearings, is measured utilizing a breakaway torque procedure described in reference 15. A shaft with high stiffness is used minimizing centrifugal growth over the range of speeds tested and directed shaft cooling is employed to limit thermal growth of the shaft diameter which would load the bearing (ref. 8). The shaft is well balanced and ground after mounting on the rig to eliminate mechanical indicated run-out. Lastly, the loading donut is statically balanced to minimize any misaligned loading of the bearing. By taking these steps, torque measured as a function of shaft speed yields data representative of foil bearings.

Results

Figure 7 plots the specific power loss versus the modified Sommerfeld number for an advanced technology, generation III bump foil air bearing operating at room temperature conditions. Table I gives the specific parameters and values used to calculate the S' and table II gives the data shown in the plot. The bearing manufacturer and general design features are described in reference 15.

The curve plotted in figure 7 is in the shape of an asymmetric parabola characterized by two distinct regimes; a highly loaded regime occurring at low values of S', and a high speed regime occurring at S' values greater than about 6. In the highly loaded regime, the specific power loss decreases approximately linearly with S'. In the high speed regime, power loss increases with S' raised to about the three-half power. At the transition between highly loaded and high speed operation, the power loss is not a strong

function of S'. Interestingly, it is observed that both regimes can yield an equivalent bearing power loss yet respond differently to changes in speed and load.

Discussion

The purpose of developing a foil bearing operating map is to be able to evaluate a foil bearing's response to a variety of variables which can be directly related to bearing and system design parameters. For instance, knowing the power loss for a specific foil bearing operating at a particular speed and load, does not indicate what might happen if the speed changes slightly. More importantly, developing a performance parameter such as S' which incorporates several key system level design variables allows one to predict or virtually test for the effects of changes without needing to conduct numerous experiments. For instance, foil bearing preload level is a common design variable used to adjust bearing stiffness and damping characteristics. In general, high preload increases stiffness, reduces dynamic shaft orbits and increases coulomb damping. However, if the bearing preload is increased, the S' is reduced and keeping all other parameters constant, bearing operation moves from the more thermally stable, lightly stressed regime towards and possibly into the more thermally unstable, highly stressed regime.

A possible explanation for this behavior is as follows. In a paper by Radil, Howard and Dykas foil bearings were tested with varying degrees of preload to evaluate load capacity and general operability (ref. 9). The authors showed that a heavily preloaded bearing was very susceptible to thermal runaway induced seizure due to high power loss. In essence, high power loss caused by high preload caused an increase in thermal expansion of the shaft into the bearing increasing spring preload even further. In the highly loaded regime of the map, increasing the loading increases the power loss (frictional heating) exacerbating thermal expansion loading and leading to seizure. The same effect occurs if the speed is reduced. With respect to the operating map, the operating point continuously moves along the curve to the left until the bearing reaches its load capacity or thermal stability limit and fails. However, if the bearing is operating in the high speed regime and the speed is decreased, the S' decreases resulting in a reduction in power loss and reverses the thermal expansion loading which allows the bearing to cool off and remain thermally stable. Figure 8 graphically shows this effect on the performance map. Based upon this assessment it is apparent that it is highly desirable to design the steady state operating points of a foil bearing supported system to fall in the high speed regime. Operating in the highly loaded regime is possible but only if adequate thermal management techniques are in place.

Interestingly, over the course of a normal start up to shut down cycle of an Oil-Free rotor system, foil bearings will operate over the entire operating map. For instance, at speeds below lift-off and prior to the development of the hydrodynamic gas film, dry sliding contact occurs and the S' value, if it were to be calculated, would be less than one. Upon lift-off, which typically occurs between one and five thousand rpm for bearings less than 100 mm in diameter, the operating point is at the far left edge of the map. To continue to operate at this point would require careful application of cooling to achieve thermal stability. As the shaft accelerates, the bearing power loss follows the curve; power loss decreases and S' increases until a minimum is reached at about an S' of 6. Figure 8 shows this effect and illustrates graphically the effects of speed and load changes on power loss.

From a purely hydrodynamics perspective, the power loss is an integral function of the friction, bearing area and shear rate. When placed in relation to the modified Sommerfeld number, S', the specific power loss is proportional to some constant divided by S'. In other words, for an S' value less than about 6, the power loss is an inverse function of the modified Sommerfeld number:

$$For \ S' \le 6,$$

$$P_l' \approx \frac{A}{S'} \tag{2}$$

The observation that the minimum power loss occurs at a value of ~6 has been verified for a variety of bearing designs, sizes and L/D ratios and represents a bearing operating at approximately 15 percent of

its load capacity. Further increases in speed beyond this point result in modest increases in power loss due to increased shear. Ideally, one would like to set the rotor system's idle speed at or slightly above an S' of 6 allowing for some margin for operating changes to prevent falling back and climbing into the highly loaded regime. Full speed operation would be set well into the high speed regime but significantly below an S' value that would push operation near the shaft burst strength limit or too close to a power loss of ~100 W/in.[2]. Again, the difference between the operating S' and an S' value that represents a change in regime (S' ≈ 6) is considered the margin.

The physics behind the shape and placement of the S' curve on the performance map is not yet fully understood. However, some aspects of the nature of the curve are not unexpected. For instance, highly loaded bearings experience a linear increase in load capacity with speed. This should approximately translate into a linear decrease in gas film shear rate, and hence friction, with speed and this is observed. Clearly, however, the existence of a power loss minimum suggests that the fluid dynamics regime changes for S' values above ~6.

It is put forth here that high speed foil gas bearing friction and power loss are dominated more by a windage mechanism than hydrodynamic shear. If the windage friction is considered dominant in this regime, a couette based approximation will yield a useful estimate of the power loss. In this case the losses are due to the shear of the gas film over the entire swept area of the bearing, not just the highly loaded region with a bearing operating at low S' values.

If it is assumed that the torque (T) and power loss for a foil bearing operating in the high speed regime is dominated by a Couette flow pattern, the following relationship can be determined.

$$T = B_1 (R_o \Omega_k)^{1/2} (W_t)^{1/2} \tag{3}$$

$$T = B_2 \sqrt{S'} \tag{4}$$

In the above relationships the square-root dependency originates from the fact that a foil journal bearing is initially preloaded again the shaft and thus must create a modest amount of hydrodynamic pressure to operate in the high speed regime. The second relation (eq. (4)) above casts the torque in the traditional Stribeck relationship of friction coefficient versus Sommerfeld number and captures the physics and nature of foil bearing experimental data in the range greater than S' of 6. The analysis can be taken an additional step to analyze specific power loss for the proposed operating map. The general form of the operating map in the high speed region can then be obtained by the following relationships.

$$P_l \approx B_3 (R_o \Omega_k)^{3/2} (W_t)^{1/2} \tag{5}$$

When S' is substituted

$$P_l \approx B(S')^{3/2} (W_t)^2 \tag{6}$$

In this case, the power loss is a fairly strong (3/2 power) function of the modified Sommerfeld number and a weak (1/2 power) function of the load. As a result, increases in speed and load lead to increased power loss. Thus depending upon the S' value, the bearing power loss will respond to speed changes differently and at low S' values, increases in load result in more significant power loss increases than at high S' values.

It is tempting to simply algebraically combine the expressions for power loss, P_l, for both highly loaded and the high speed operating regimes in the same expression and plot them on a simple P_l versus S' plot. This cannot be accomplished with theoretical rigor, however, unless the load is held constant.

Since S' includes both load and speed, changes in operating load affect both the S' and the power loss and is not independent. For this preliminary study, graphing of the data will be restricted to tests at constant load. Figure 7 shows such a plot of power loss versus S' for a fixed load. Essentially, this is a plot of power loss versus speed. For this particular case, a curve fitting routine was conducted to determine the constants and the equation is shown below and in figure 9.

$$P_l = \frac{A}{S'} + B(S')^{3/2}(W_t)^2 \tag{7}$$

Exploratory tests of bearings operating at a constant high speed in which only the load was perturbed, indicate that the power loss is proportional to the load raised to the one-half power which is consistent with equation (7). This indicates that a three dimensional or parametric type plot utilizing perhaps, speed (Ω), load (w) and power loss (P_l), would be most appropriate. In this case, a series of power loss curves at various loads will describe a response surface or carpet type plot on which differing operating points and the paths between them can be adequately shown.

More research will be required to investigate whether the constants in equation (7) are universal or bearing specific. Also, as described in an earlier section, an increased directional load, such as heavy deadweight addition, will deflect the bearing housing in the direction of the load reducing more distributed loads, such as spring preload, opposite this direction. This load shifting may make the relationship between discrete loads and the total specific load incorporated in the S' parameter a complex and yet to be determined function.

Further exploration of the S' parameter reveals that it can be used to achieve robust foil bearing supported systems. For instance, the load capacity coefficient, $\mathcal{D}$, has a direct effect on the maximum S' that can be attained. If a low technology, simple design Generation I bearing is employed with a coefficient of only 0.25, the operating space for the system is compressed and hence the operating margins are reduced. Similarly, factors which increase the total bearing load (W_t) such as high preload levels, excessive thermal and centrifugal expansion of the shaft and dynamic loads all contribute to low levels of S'. Even at high shaft speeds, excessive total load (W_t) may result in shifting the operating point from "safe" operation above an S' of 6 to less desirable operation in the highly loaded region. In addition, the S' parameter helps explain why simply installing a larger diameter bearing may not significantly improve operating margins. Larger diameter shafting generally results in higher centrifugal shaft expansion essentially increasing the load on the bearing.

Clearly, the path to improving system level robustness is to utilize bearings with the highest load capacity coefficient available; sophisticated Generation III bearings with performance coefficients of 1.0. Designing shafting with high structural stiffness, good thermal conductivity and free from mechanical run-out also result in margin gains. Minimizing spring preloading and paying particular attention to thermal management of both the shaft and the bearing are also essential to a thermally stable system. Lastly, the creation of a foil bearing operating map for the bearing under consideration is a valuable tool to determine the relative importance of the other parameters of the system such as operating speeds, rotor weights and other factors.

Summary

A new foil bearing operating map is introduced to assist in the application of foil gas bearings to high speed rotor systems. This map combines classical hydrodynamic understanding articulated through the Stribeck Curve with empirically based foil gas bearing performance characteristics to yield a useful tool for designing new systems. Since thermal management is a dominant factor in foil bearing operating health, it is used as a primary measurand of the map. The second measureand is a highly modified form of the Sommerfeld number, S', which relates the gas pressure generated in the film to the total unit load supported by the bearing. Thus, the S' represents an inverse bearing stress or severity factor. S' is readily

calculated and incorporates environmental, bearing design, and system level parameters. In this fashion, the operating map provides a valuable tool for bearing research and development as well as guidance in integrating foil bearings into rotor support systems.

Preliminary theoretical analyses suggest that the power loss curve behaves as a polynomial supposition of linear and non-linear factors. Highly loaded bearings exhibit power loss in an inverse relation to S' and high speed bearings exhibit power loss with S'$^{3/2}$ W^2. More work will be needed to refine these analyses and much more experimentation is needed to establish the values for the proposed constants. The good agreement with basic hydrodynamic theory and the initial experimental results suggest that the approach presented here is reasonable.

Though just in the preliminary stage, the operating map serves as a useful method for understanding the system factors such as load, speed and size on bearing performance. More importantly, the map readily illustrates how much of a safety margin exists at any given system operating point. As a supplement to the results of the four step development method, the information resulting from the proposed operating map can be used to design a robust system which can be tolerant to off-design conditions. Finally, it is expected that this operating map concept will evolve as more experimental data and more analytical understanding of foil bearings becomes available.

References

1. Heshmat, H., Shapiro, W., and Gray, S., "Development of Foil Journal Bearings for High Load Capacity and High Speed Whirl Stability," Transactions of the ASME Journal of Lubrication Technology, volume 104, number 2, pp. 149–156, April 1982.
2. DellaCorte, C. and Valco, M.J., "Oil-Free Turbomachinery Technology for Regional Jet, Rotorcraft, and Supersonic Business Jet Propulsion Engines," Proceedings of the 2003 International Society of Airbreathing Engines Conference, Cleveland, Ohio, September 2003, ISABE Paper #2003-1182.
3. Suriano, F.J., "Gas Foil Bearing Development Program," U.S. Airforce Report #AFWAL-TR-81-2095.
4. Valco, M.J. and DellaCorte, C., "Emerging Oil-Free Turbomachinery Technology for Military Propulsion and Power Applications," Proceedings of the ARMY Sciences Conference, Ft. Lauderdale, FL, February, 2003.
5. DellaCorte, Christopher and Valco, Mark J., "Load Capacity Estimation of Foil Air Journal Bearings for Oil-Free Turbomachinery Applications," Tribology Transactions, Vol. 43, Number 4, pp. 795–801, October 2000.
6. Dykas, B. and Howard, S.A., "Journal Design Considerations for Turbomachine Shafts Supported on Foil Air Bearings," Tribology Transactions, vol. 47, no. 4, 2004, pp. 508–516.
7. Salehi, M., Swanson, E., and Heshmat, H., "Thermal Features of Compliant Foil Bearings-Theory and Experiment," Journal of Tribology, Volume 123, Issue 3, July 2001, pp. 566–571.
8. Radil, K.C. and Zeszotek, M., "An Experimental Investigation Into the Temperature Profile of a Compliant Foil Air Bearing," NASA/TM—2004-213100, May 2004.
9. Radil, K.C., Howard, S.A., and Dykas, B., "The Role of Radial Clearance on the Performance of Foil Air Bearings," NASA/TM—2002-211705.
10. Hill, P.G. and Peterson, C.R., "Mechanics and Thermodynamics of Propulsion," second edition, Addison-Wesley Publishing Company, Reading, Massachusetts, 1992, pp. 453.
11. Lu, X. and Khonsari, M.M., "On the Lift-off speed in journal bearings," Tribology Letters, volume 20, numbers 3-4, December 2005, pp. 299–305.
12. DellaCorte, Christopher and Pinkus, Oscar, "Tribological Limitations in Gas Turbine Engines a Workshop to Identify the Challenges and Set Future Directions," NASA/TM—2000-210059, May 2000.
13. Dykas, B.D., Prahl, J.M., Bruckner, R.J., and DellaCorte, C., "Thermal Management Phenomena in Thrust Foil Gas Bearings," presented at the 2006 ASME IGTI, Barcelona, Spain, May 2006, paper number GT2006-91268.
14. DellaCorte, Christopher, "A New Foil Air Bearing Test Rig for Use to 700 °C and 70,000 rpm," NASA TM–107405, Prepared for the 1997 Tribology Conference cosponsored by the Society of

Tribologists and Lubrication Engineers and the American Society of Mechanical Engineers, London, England, UK, September 8–12, 1997. Tribology Transactions, Vol. 41, pp. 335–340, July 1998.

15. DellaCorte, Christopher, Lukaszewicz, V.L., Valco, M.J., Radil, K.C., and Heshmat, H. "Performance and Durability of High Temperature Foil Air Bearings for Oil-Free Turbomachinery," NASA/TM— 1999-209187, November 1999. Tribology Transactions, Vol. 43, Number 4, pp. 774–780, October 2000.

16. Heshmat, H., "High Load Capacity Compliant Foil Hydrodynamic Journal Bearing," U.S. Patent # 5,988,885, November 23, 1999.

TABLE I.—PARAMETERS AND VALVES FOR
BEARING FRICTION TESTS

Parameter	Value
Bearing style	Gen III bump foil
Diameter	2.0 in. (50 mm)
Length	2.0 in. (50 mm)
Load capacity, coef $\mathcal{D}$	≈ 1.0 lb/in.^{3} krpm
Spring preload	≈ 0.50 psi (750 kPa)
Manufacturer	Mohawk innovative technology
Patent number	5,988,885

TABLE II.—TYPICAL BEARING POWER LOSS DATA
USED FOR GENERATING OPERATING MAP

Speed, krpm	Total load, lbs (N)	Projected area, L×D (in.^{2})[mm^2]	Torque, N-m	Specific power loss, W/in.^{2} (W/mm^2)	S'
0	11.5 (52)	2×2 (4) [2581]	0.000	0	0.0
5			.303	40	3.4
6			.221	35	4.2
7			.138	25	4.9
8			.095	20	5.5
9			.051	12	6.2
10			.041	11	7.0
11			.033	9.7	7.7
12			.027	8.5	8.3
13			.025	8.6	9.0
14			.025	9.0	9.8
15			.024	9.6	10.4
20			.026	13.7	15.8
30			.031	25	20.9
40			.041	43	27.8
50	11.5 (56)	2×(4)[2581]	.051	66	34.8

[a]$\mathcal{D}$ = 1.0 lb/in.^{3}/Krpm, L = 2.0 in., D = 2.0 in.
Deadweight = 5.2 lb (23 N)
Spring preload = 0.5 psi $\Rightarrow$ 6.3 lb (28 N)
Tests conducted at 25 °C with 6 scfm cooling air, directed at shaft inside diameter
Bearing design described in (ref. 16)
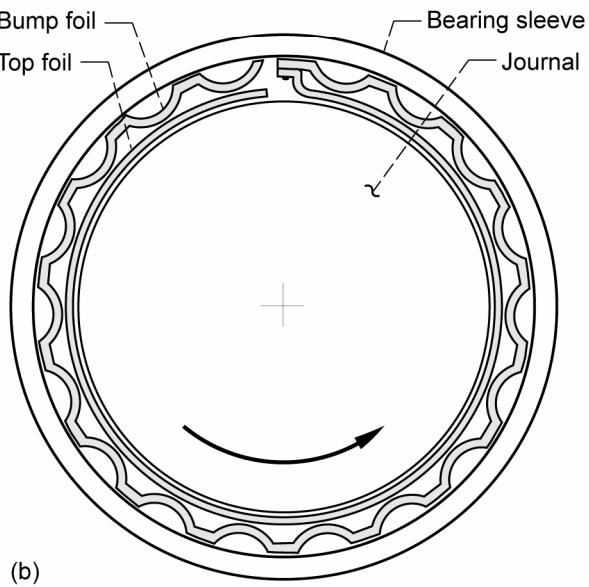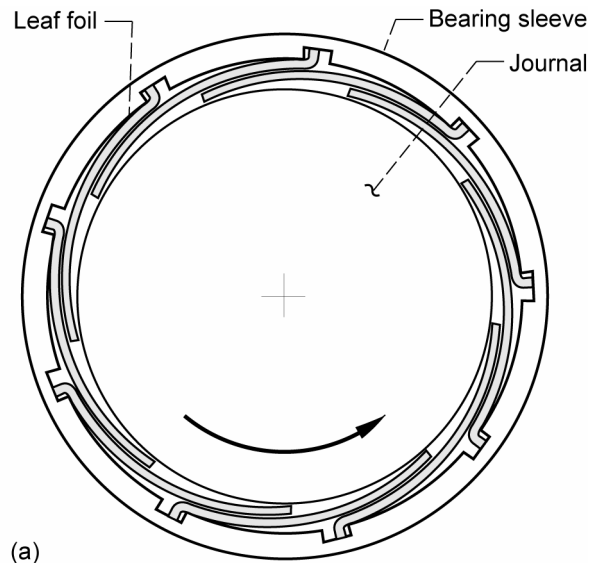
Figure 1.—Early foil bearing designs. (a) Leaf-type foil bearing. (b) Bump-type foil bearing.
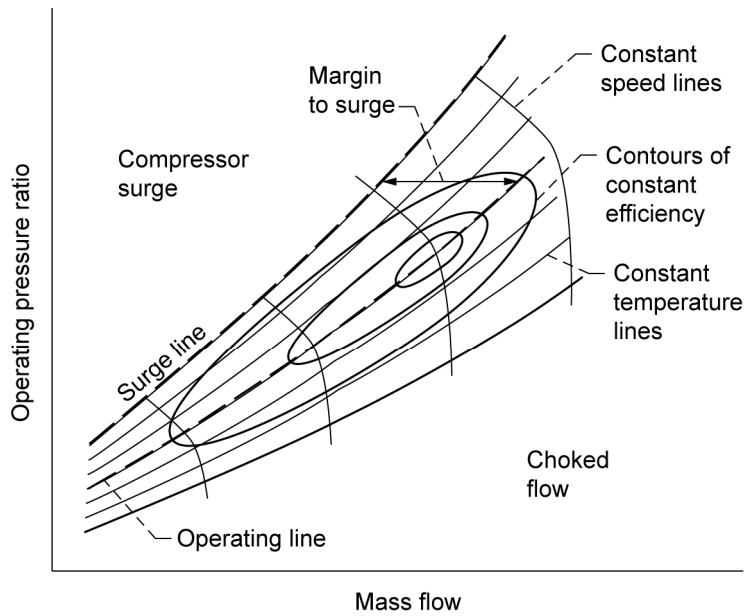
Figure 2.—Typical turbocompressor operating map showing flow regions, safe operating points, and efficiency adapted from (ref. 10).
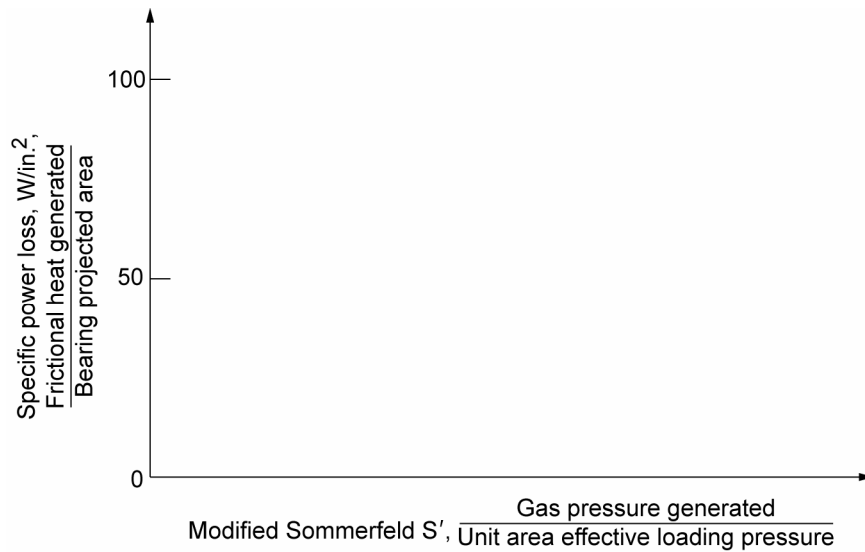

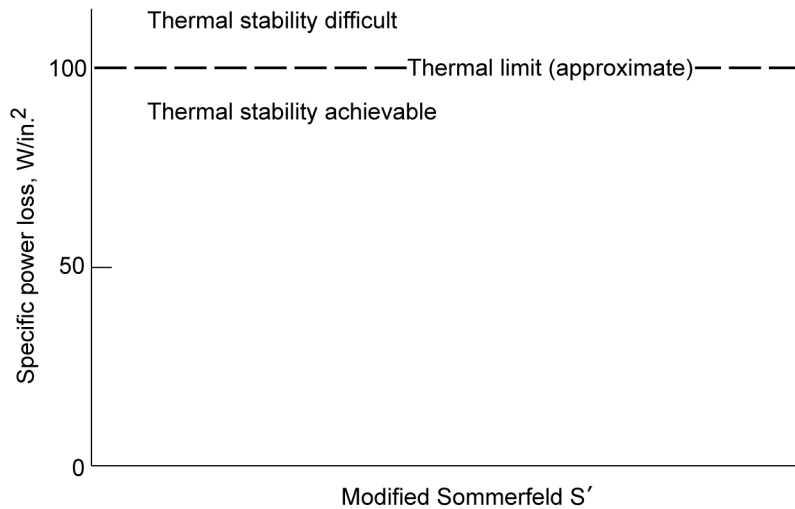Figure 3.—Foil bearing operating map axes.

Figure 4.—Foil bearing operating map axes (thermal limit at ≈ 100 W/in.^{2}).

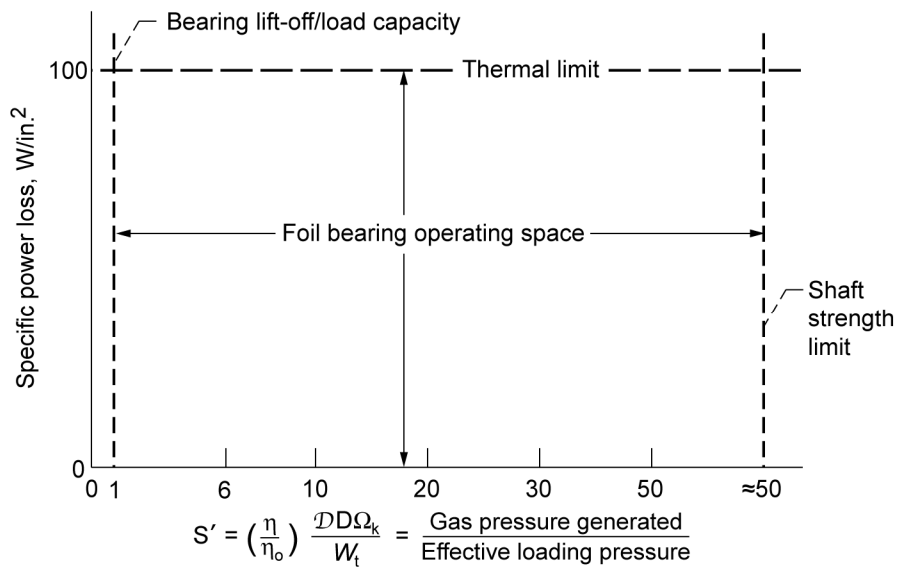$$S' = \left(\frac{\eta}{\eta_o}\right) \frac{\mathcal{D}D\Omega_k}{W_t} = \frac{\text{Gas pressure generated}}{\text{Effective loading pressure}}$$

Figure 5.—Foil bearing operating map showing physical limits to operating space.
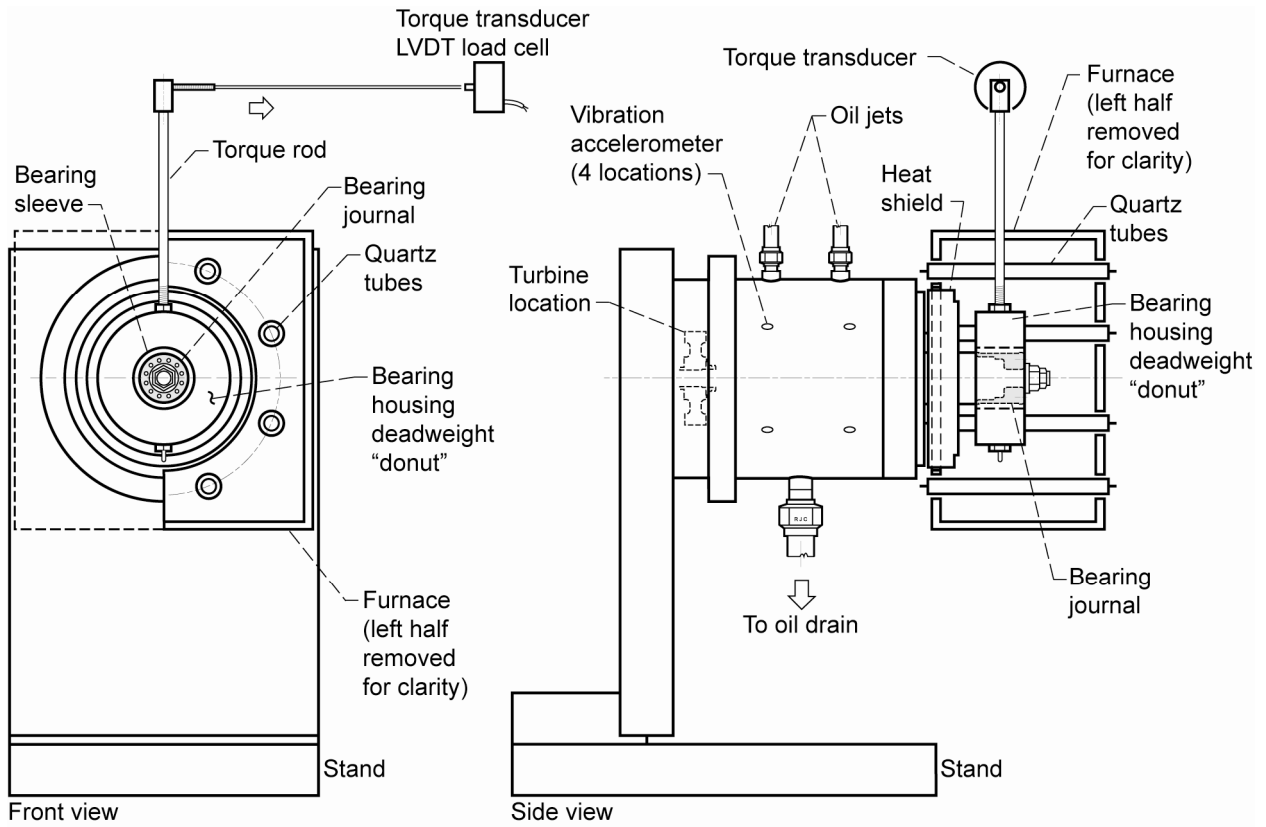
Figure 6. —Schematic view of high-temperature, high-speed foil bearing test rig used to measure bearing power loss.
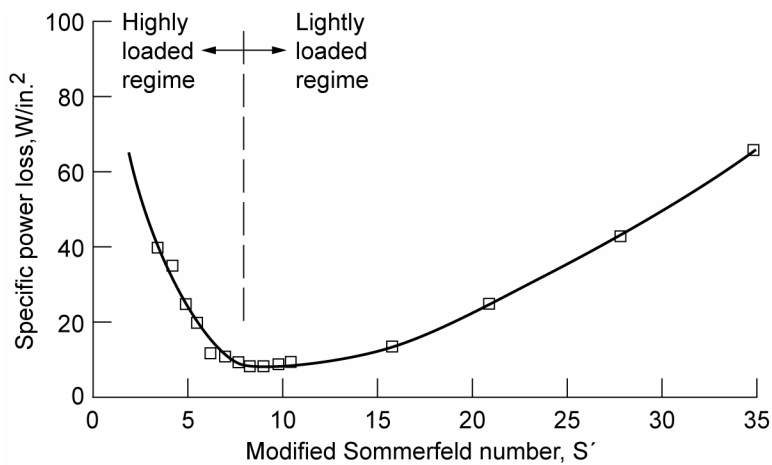
Figure 7.—Foil bearing operating map for 50 mm diameter, 50 mm long (Generation III - ref. 16) journal bearing operating at room temperature. Data from table II.
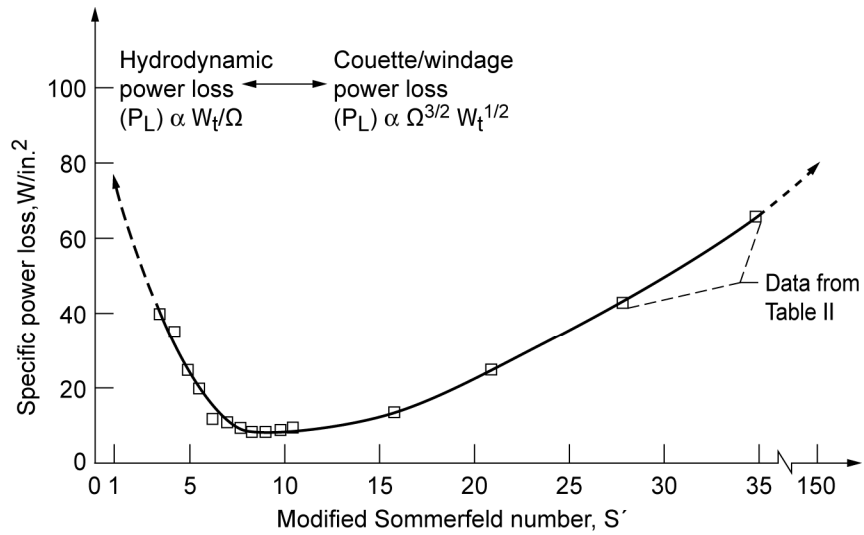
Figure 8.—The effects of S´ (load and speed) changes on the thermal stability and operating regime of a foil journal bearing. At high S´ values, decreases in speed and load reduce thermal stresses. At low S´ values, decreases in speed and increases in load increase thermal stresses.
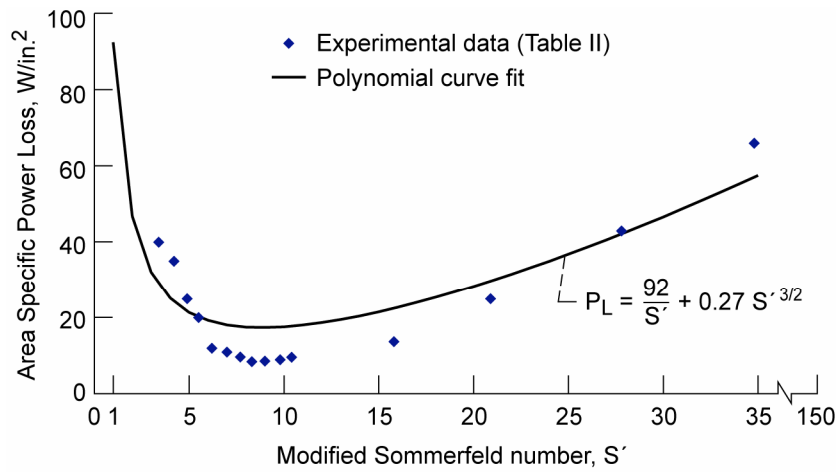
Figure 9.—Experimental data and polynomial curve-fit of the mathematical relationship for specific power loss as a function of modified Sommerfeld S´ and load.

REPORT DOCUMENTATION PAGE

1. AGENCY USE ONLY (Leave blank)	2. REPORT DATE	3. REPORT TYPE AND DATES COVERED
	October 2006	Technical Memorandum

4. TITLE AND SUBTITLE

A Preliminary Foil Gas Bearing Performance Map

5. FUNDING NUMBERS

WBS 561581.02.07.03.03.02

6. AUTHOR(S)

Christopher DellaCorte, Kevin C. Radil, Robert J. Bruckner, and S. Adam Howard

7. PERFORMING ORGANIZATION NAME(S) AND ADDRESS(ES)

National Aeronautics and Space Administration
John H. Glenn Research Center at Lewis Field
Cleveland, Ohio 44135–3191

8. PERFORMING ORGANIZATION REPORT NUMBER

E–15569

9. SPONSORING/MONITORING AGENCY NAME(S) AND ADDRESS(ES)

National Aeronautics and Space Administration
Washington, DC 20546–0001
and
U.S. Army Research Laboratory
Adelphi, Maryland 20783–1145

10. SPONSORING/MONITORING AGENCY REPORT NUMBER

NASA TM—2006-214343
ARL–TR–3902

12a. DISTRIBUTION/AVAILABILITY STATEMENT

Unclassified - Unlimited
Subject Category: 37

Available electronically at http://gltrs.grc.nasa.gov

This publication is available from the NASA Center for AeroSpace Information, 301–621–0390.

12b. DISTRIBUTION CODE

13. ABSTRACT (Maximum 200 words)

Recent breakthrough improvements in foil gas bearing load capacity, high temperature tribological coatings and computer based modeling have enabled the development of increasingly larger and more advanced Oil-Free Turbomachinery systems. Successful integration of foil gas bearings into turbomachinery requires a step wise approach that includes conceptual design and feasibility studies, bearing testing, and rotor testing prior to full scale system level demonstrations. Unfortunately, the current level of understanding of foil gas bearings and especially their tribological behavior is often insufficient to avoid developmental problems thereby hampering commercialization of new applications. In this paper, a new approach loosely based upon accepted hydrodynamic theory, is developed which results in a "Foil Gas Bearing Performance Map" to guide the integration process. This performance map, which resembles a Stribeck curve for bearing friction, is useful in describing bearing operating regimes, performance safety margins, the effects of load on performance and limiting factors for foil gas bearings.

14. SUBJECT TERMS

Bearings; Gas; Foil; Hydrodynamics; Tribology; Friction measurements; Aerospace; High temperatures; Turbomachinery

15. NUMBER OF PAGES

21

16. PRICE CODE

17. SECURITY CLASSIFICATION OF REPORT	18. SECURITY CLASSIFICATION OF THIS PAGE	19. SECURITY CLASSIFICATION OF ABSTRACT	20. LIMITATION OF ABSTRACT
Unclassified	Unclassified	Unclassified	